

# Wind Tunnel Testing of High Efficiency Low Power (HELP) Actuation for Active Flow Control

John C. Lin<sup>\*</sup>, Latunia P. Melton<sup>†</sup>, Judith A. Hannon<sup>‡</sup>, Marlyn Y. Andino<sup>§</sup>,  
Mehti Koklu<sup>\*\*</sup>, Keith B. Paschal<sup>††</sup>, and Veer N. Vatsa<sup>‡‡</sup>

*NASA Langley Research Center, Hampton, VA, 23681, USA*

A High Efficiency Low Power (HELP) methodology has been successfully developed and tested on an active flow control (AFC) version of the 10%-scale high-lift Common Research Model (CRM-HL) at the NASA Langley Research Center 14- by 22-Foot Subsonic Tunnel (14x22). The AFC variant of the CRM-HL, designated as CRM-SHL-AFC, was integrated with modular HELP actuator cartridges on the shoulder of its highly deflected ( $\geq 50^\circ$ ) simple-hinged flaps. A reference conventional CRM-HL configuration equipped with Fowler flaps and a nacelle chine was chosen to provide the targeted lift enhancement goals and for comparison with the results of the CRM-SHL-AFC. The current data are presented with the Transonic Wall Interference Correction System (TWICS) method applied. The HELP actuators, which use a combination of unsteady sweeping jets and steady discrete jets in tandem, were designed to overcome strong adverse pressure gradients, while minimizing the pneumatic power usage. The power coefficient ( $C_\pi$ ), which takes account of both supply air pressure and mass flow usage for the AFC actuators, is a useful parameter for judging the actuators' performance efficiency and perhaps for scaling-up of the AFC system. Full HELP actuation coverage with a constant spanwise nozzle pressure ratio (NPR) was able to achieve the lift enhancement goals for the entire lift curve and was found to be the most effective AFC case. For the most effective case, mass flow rates greater than  $\sim 0.91$  lbm/s and NPR values greater than  $\sim 1.8$  (corresponding to  $C_\pi = 0.18$ ) are needed to achieve the lift enhancement goal at  $\alpha = 9^\circ$ , whereas mass flow rates greater than  $\sim 1.23$  lbm/s and NPR values greater than  $\sim 2.3$  (corresponding to  $C_\pi = 0.3$ ) are needed to achieve the lift enhancement goal at  $\alpha = 17^\circ$ . Surface pressure distributions indicate that the HELP actuation on the flap shoulder increased the suction pressures (and flow circulation) globally in both the streamwise and the spanwise directions, and thereby enhanced the lift over the entire high-lift system. The CRM-SHL-AFC configuration equipped with HELP actuation was able to match or exceed the lift performance of the reference conventional CRM-HL, thus meeting the objective of the research.

## I. Nomenclature

$A_n$	=	total area of all active nozzle exits
$c_r$	=	mean aerodynamic chord; 27.58 inches
$C_D$	=	drag coefficient; (drag force)/( $S \cdot q_\infty$ )
$C_L$	=	lift coefficient; (lift force)/( $S \cdot q_\infty$ )
$C_m$	=	pitching moment coefficient; (pitching moment)/( $S \cdot c_r \cdot q_\infty$ )
$C_p$	=	pressure coefficient; $(p - p_\infty)/q_\infty$
$C_Q$	=	mass flow coefficient; $\dot{m}/(\rho_\infty \cdot S \cdot U_\infty)$
$C_\mu$	=	momentum coefficient; $\dot{m}^2/(\rho_n \cdot A_n \cdot q_\infty \cdot S)$

---

<sup>\*</sup> Senior Research Scientist, Flow Physics and Control Branch, MS 170, AIAA Associate Fellow

<sup>†</sup> Senior Research Scientist, Flow Physics and Control Branch, MS 170, AIAA Associate Fellow

<sup>‡</sup> Research Scientist, Flow Physics and Control Branch, MS 170

<sup>§</sup> Research Scientist, Flow Physics and Control Branch, MS 170, AIAA Senior Member

<sup>\*\*</sup> Research Scientist, Flow Physics and Control Branch, MS 170

<sup>††</sup> Research Scientist, Flow Physics and Control Branch, MS 170

<sup>‡‡</sup> Senior Research Scientist, Computation AeroSciences Branch, MS 128, AIAA Associate Fellow

$C_\pi$	=	power coefficient; $(C_Q \cdot P_a)/q_\infty$
$\dot{m}$	=	total mass flow rate
$M_\infty$	=	freestream Mach number
$p$	=	pressure
$p_\infty$	=	freestream static pressure
$P_a$	=	actuator plenum pressure
$q_\infty$	=	freestream dynamic pressure
$Re_c$	=	Reynolds number based on mean aerodynamic chord ( $c_r$ )
$S$	=	wing reference area
$U_\infty$	=	freestream velocity
$x, y, z$	=	coordinates along the model's longitudinal axis, lateral axis, and normal axis, respectively
$\alpha$	=	angle of attack
$\Delta C_L$	=	lift coefficient increment
$\rho_\infty$	=	freestream density
$\rho_n$	=	air density at the actuator nozzle

## II. Introduction

A modern high-lift system is typically designed to allow a transport aircraft — with transonic cruise speeds — to safely operate at slow speeds for landing and takeoff operations. The high-lift system is usually slotted both on the leading edge and the trailing edge of the wing to take advantage of the aerodynamic properties of slotted flows and achieve the necessary high-lift performance [1]. However, the slotted trailing-edge devices such as the Fowler flaps and the associated subsystems necessary to change the wing configuration from cruise to low-speed, are complex and protrude externally under the wings — and require external fairings — that result in increased cruise drag. One possible approach to mitigate this issue is to use simple-hinged flaps with active flow control (AFC) [2,3] to provide the required high-lift performance while reducing the associated external drag.

Simple-hinged flaps are the most basic flaps due to their simple design and operation; however, they often require higher flap deflections (i.e.,  $> 40^\circ$ ) than other more complex flap designs [4-6]. The purpose of such high flap deflections is to increase the wing camber such that it would have the potential to achieve aerodynamic lift performance comparable to a conventional Fowler (slotted) flap high-lift system, while eliminating the cruise drag penalty associated with the external deployment mechanism for the Fowler flap systems. System integration studies indicated that up to a 2.25% fuel burn reduction is possible if an AFC-enabled simplified high-lift system (i.e., simple-hinged flaps inboard and outboard) could provide the equivalent lift level as the one equipped with a Fowler flap system [5]. However, the high flap deflection on the simple-hinged flap produces strong adverse pressure gradients, and hence massive flow separation on the flap that is extremely challenging to attenuate using AFC methods. A novel AFC concept, namely the High Efficiency Low Power (HELP) methodology, has been developed for simple-hinged flap high-lift systems [7]. The HELP actuation methodology overcomes this challenging problem and makes the simple-hinged flap systems a possible option for future aircraft designs.

Under the sponsorship of the NASA Advanced Air Transport Technology (AATT) Project, a 10%-scale conventional high-lift version of the Common Research Model (CRM-HL) and an Active Flow Control (AFC) version of the model equipped with a simple-hinged flap (CRM-SHL-AFC) [7-10] were successfully tested at the NASA Langley Research Center 14- by 22-Foot Subsonic Tunnel (14x22). The wind tunnel test demonstrated that the HELP actuators were extremely effective in controlling the massive flow separation on the CRM-SHL-AFC with high flap deflections ( $\geq 50^\circ$ ). The HELP actuators were the only AFC actuators examined during the test that met or exceeded the targeted lift performance goal. The HELP actuation concept may represent a breakthrough in flow separation control technology because it can be used to achieve lift enhancement more efficiently by using less pneumatic power compared to other flow control techniques such as circulation control [11].

This paper presents the 14x22 test results of the CRM-SHL-AFC using the HELP actuators in detail, which include the AFC parameters such as actuator coverage, nozzle pressure ratio (NPR), mass flow, and pneumatic power usage. Furthermore, a flow physics analysis based on surface pressure and flow visualization is also presented in the paper.

### III. Wind Tunnel Test

The wind tunnel test was performed at the NASA Langley Research Center (LaRC) 14- by 22-Foot Subsonic Tunnel (14x22) [12]. The 14x22 is an atmospheric, closed return wind tunnel with a 14.5-ft high, 21.75-ft wide, and 50-ft long test section. When testing in the closed-wall configuration, a maximum freestream velocity of 338 ft/s and a dynamic pressure ( $q_\infty$ ) of 144 psf can be achieved. The unit Reynolds number ranges from 0 to  $2.2 \times 10^6$  per foot. A 10%-scale semispan (right wing) CRM-HL was fabricated and tested in the landing configuration at a nominal freestream Mach number ( $M_\infty$ ) of 0.2 with a corresponding  $q_\infty$  of approximately 60 psf and a Reynolds number based on mean aerodynamic chord ( $Re_c$ ) of  $3.27 \times 10^6$ .

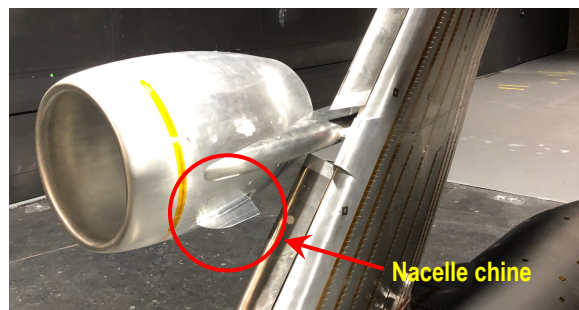
The experimental measurements included forces and moments using a balance (NASA MC-110), surface static pressures using pressure taps and electronically scanned pressure (ESP) modules, surface dynamic pressures using unsteady pressure sensors (Kulites®), as well as flow visualization using minitufts [10] and infrared (IR) cameras. Based on the balance accuracy, angle of attack ( $\alpha$ ) and  $q_\infty$ , the expected instrumentation uncertainty is estimated to be within  $\pm 0.01$  for the lift coefficient ( $C_L$ ),  $\pm 0.0030$  to  $\pm 0.0040$  for the drag coefficient ( $C_D$ ), and  $\pm 0.0030$  to  $\pm 0.0035$  for the pitching moment coefficient ( $C_m$ ). The uncertainty of the latter two is also a function of  $\alpha$  — i.e., a greater uncertainty is associated with higher angles of attack.

#### A. Wind Tunnel Model Configurations: CRM-HL (Reference Case) and CRM-SHL-AFC

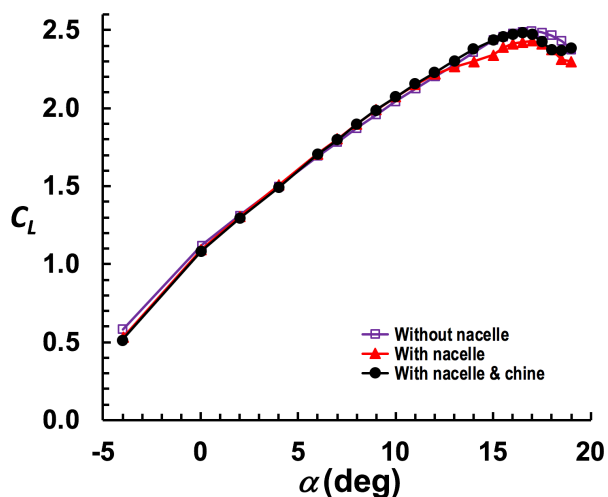
The current high-lift research effort involves a reference conventional high-lift configuration (CRM-HL) that is based on the open NASA Common Research Model (CRM) [13-15]. The CRM-HL configuration was reported by Lacy and Sclafani [16] and it is intended to be open as well. Detailed descriptions of the 10%-scale CRM-HL model features were reported in Lin et al. [7]. A photo of the semispan CRM-HL installed vertically in the 14x22 is shown in the Fig. 1(a).



(a) Reference CRM-HL in the 14x22



(b) Chine installation on the nacelle



(c) Nacelle chine fixed a prestall lift degradation [7] (no wall correction applied to  $\alpha$ )

Fig. 1 Reference CRM-HL.

Aerodynamic performance data of the conventional high-lift configuration (CRM-HL) with a  $30^\circ$  slat deflection, a  $37^\circ$  flap deflection, and a nominal slat and flap position setting as reported by Lacy and Sclafani [16] were acquired

as part of the test campaign at the 14x22. The CRM-HL lift performance provides a target for the CRM-SHL-AFC configuration to achieve. In order to represent a typical modern high-lift system, all test runs were performed with a wing/fuselage strake (or filler) and the engine nacelle attached to the model. The installation of a nacelle chine (Fig. 1(b)) was needed to resolve a prestall lift performance degradation issue for the CRM-HL (Fig. 1(c)). The results of this CRM-HL configuration with the nacelle chine was selected to provide the targeted lift enhancement goals and to serve as the reference for comparison with those of the CRM-SHL-AFC [7]. Notice that the CAD for an earlier CRM-HL configuration without the nacelle, wing/fuselage strake, and brackets can be downloaded from the AIAA High-Lift Prediction Workshops website [17].

The AFC-enabled high-lift configuration (CRM-SHL-AFC) equipped with 50° inboard and 55° outboard (50°/55°) simple-hinged flaps was also built and tested at the 14x22 [7]. The outboard flap deflection was higher but necessary to align the outboard edge of the inboard flap with that of the inboard edge of the outboard flap. The 30° slat and most of the main wing, with the exception of the trailing edge/cove components, are the same between the AFC-enabled and the conventional high-lift geometries. The inset sketch in Fig. 2 illustrates the difference between the two configurations with a sectional view across the midspan of the outboard flap.

A schematic of the pressure tap locations, indicated by dots, is also shown in Fig. 2. Most of the pressure taps are in streamwise arrays at eight spanwise locations with three rows across the inboard flap span, three rows across the outboard flap span, and two rows across the aileron region — i.e.,  $y = 17.45, 27.75, 38.05, 48.35, 63.8, 79.25, 94.7,$  and 105 inches; where the yehudi break that separates the inboard and outboard flaps is located at  $y = 42.8$  inches. Pressures from three of these rows at  $y = 27.75$  inches (across the midspan of the inboard flap),  $y = 63.8$  inches (across the midspan of the outboard flap or near the midspan of the model), and  $y = 94.7$  inches (beyond the outboard flap), as identified in Fig. 2, are selected for analysis later in this paper. Additionally, six spanwise arrays are on the upper wing surface with one row on the slat, three rows on the main wing, and two rows on the flap. The total number of pressure taps on the wing is 611. Other locations for pressure taps include the fuselage (56) and nacelle/pylon (63). There are 31 unsteady pressure sensors installed on the model that include six on the wingtip, seven on the pylon, six on the outboard edge of the conventional flap, and twelve on the simple-hinged flap (six each on the inboard and the outboard flaps). There are also four accelerometers installed inside the main wing.

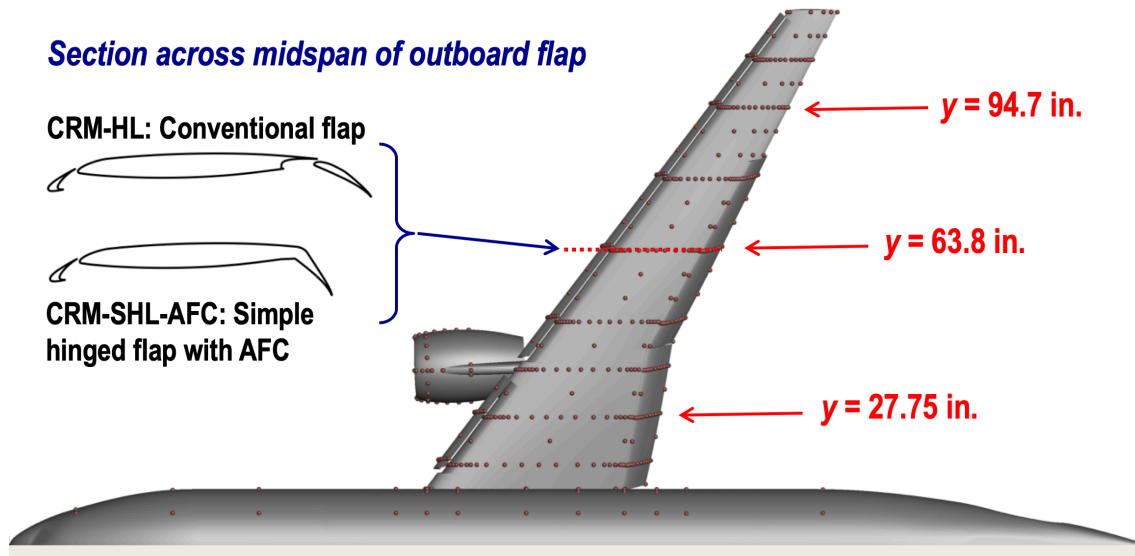


Fig. 2 Schematic of pressure tap locations and representative cross section of high-lift configurations.

### B. HELP actuators

The HELP actuation is a new and promising flow-control approach that combines unsteady sweeping jet blowing [18] for Row 1 and steady discrete jet blowing for Row 2 (see Fig. 3). The purpose of the HELP actuator's design is to enable the sweeping jet actuators of Row 1 to emit a significantly smaller amount of mass flow than that of the discrete jets of Row 2, and therefore, effectively precondition the boundary layer such that the Row 2 actuators can achieve much better flow control

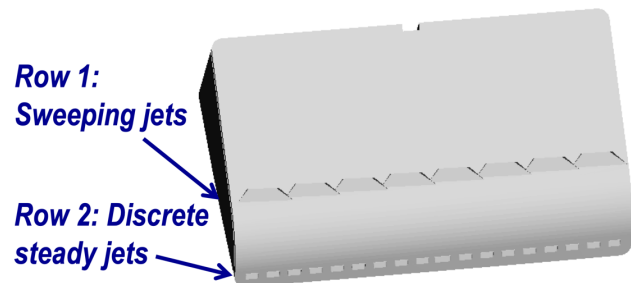
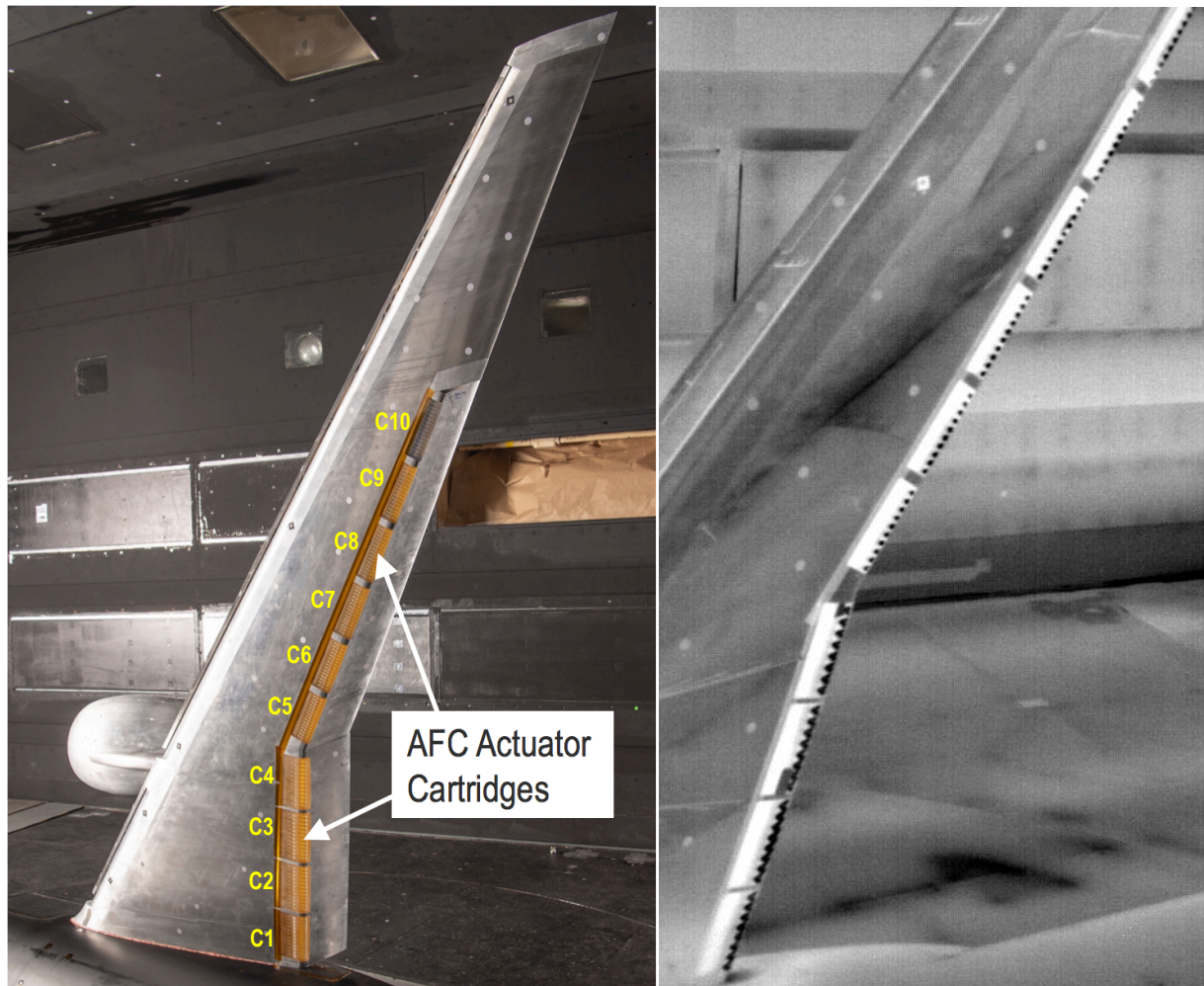


Fig. 3 HELP actuator cartridge.

authority. The intended goal of the boundary-layer preconditioning is to attenuate the effects of the surface curvature and the adverse pressure gradient at the flap shoulder. The design also leverages the synergistic benefit of allowing the two rows of actuators to act together to produce a total aerodynamic lift that is greater than the sum of each row acting individually. The HELP actuation concept is designed to expand the range of flow separation control in the linear region of the lift versus mass flow curves, which also makes the HELP actuation highly efficient.

The installation of the HELP actuator cartridges on the flap shoulder of the CRM-SHL-AFC (4 inboard and 6 outboard) is shown in Fig. 4(a). The cartridges are enumerated in sequential order, where the most inboard cartridge is designated as C1 and most outboard one is designated as C10. The IR cameras are used for functional/health monitoring of HELP actuators during each run, as shown by an example in Fig. 4 (b). The actuator cartridges are made of plastic, and therefore, show up as a lighter color in the image. The cooler jets exiting the actuators show up as a dark color. The zigzag pattern of the jet flow is due to the spreading sweeping jets in Row 1. Notice that the discrete jets of Row 2 are out of view in the image of Fig. 4(b).



(a) AFC installation on CRM-SHL-AFC

(b) Example of an IR image of HELP actuators  
(NPR = 2.4,  $\alpha = 9^\circ$ ,  $M_\infty = 0.2$ )

Fig. 4 CRM-SHL-AFC in the 14x22 and HELP actuators.

There are five control valves on a pressure manifold inside the model fuselage and each valve controls a pair of hoses for supplying pressurized air to the ten AFC cartridges. The plenum pressure and mass flow rate for the cartridges could be varied by the control valves and/or by an individual actuator exit being physically plugged. The AFC test parameters investigated include mass flow rate (up to nearly 1.4 lbm/s), nozzle pressure ratio (up to 3), and actuation coverage in the spanwise direction.

## V. Results and Discussion

The results presented in this paper are with tunnel wall corrections applied using the Transonic Wall Interference Correction System (TWICS) method [19-21]. Previous CRM-HL test results presented [7-10] had no wall correction applied. The wall correction method uses measured wall pressures and takes account of solid body blockage, separation wake blockage, and lift interference correction for a semispan model.

The application of TWICS typically increased the angle of attack ( $\alpha$ ) for the lift curve by  $0.2^\circ$  to  $1.2^\circ$  and decreased the maximum lift coefficient by  $\sim 0.01$  to  $0.06$ , as illustrated in Fig. 5 for the reference CRM-HL and the baseline (AFC off) cases.

The wind tunnel test results and discussion are presented in the following three subsections: (A) Aerodynamic Performance, (B) Pneumatic Power Usage, and (C) Surface Pressures and Flow Visualization.

### A. Aerodynamic Performance

The HELP actuation demonstrated that it could provide a very strong flow control authority as intended. The synergistic benefit, which results from the two rows actuating together to produce a lift that is greater than the sum of each row actuating individually, is clearly illustrated in the lift curves of Fig. 6. This effect is much more pronounced at higher angles of attack where the adverse pressure gradient is stronger. By design, the sweeping jets of Row 1 discharge a small amount of the mass flow to enable the discrete jets of Row 2 to have greater flow control authority, effectively boosting the Coanda effect.

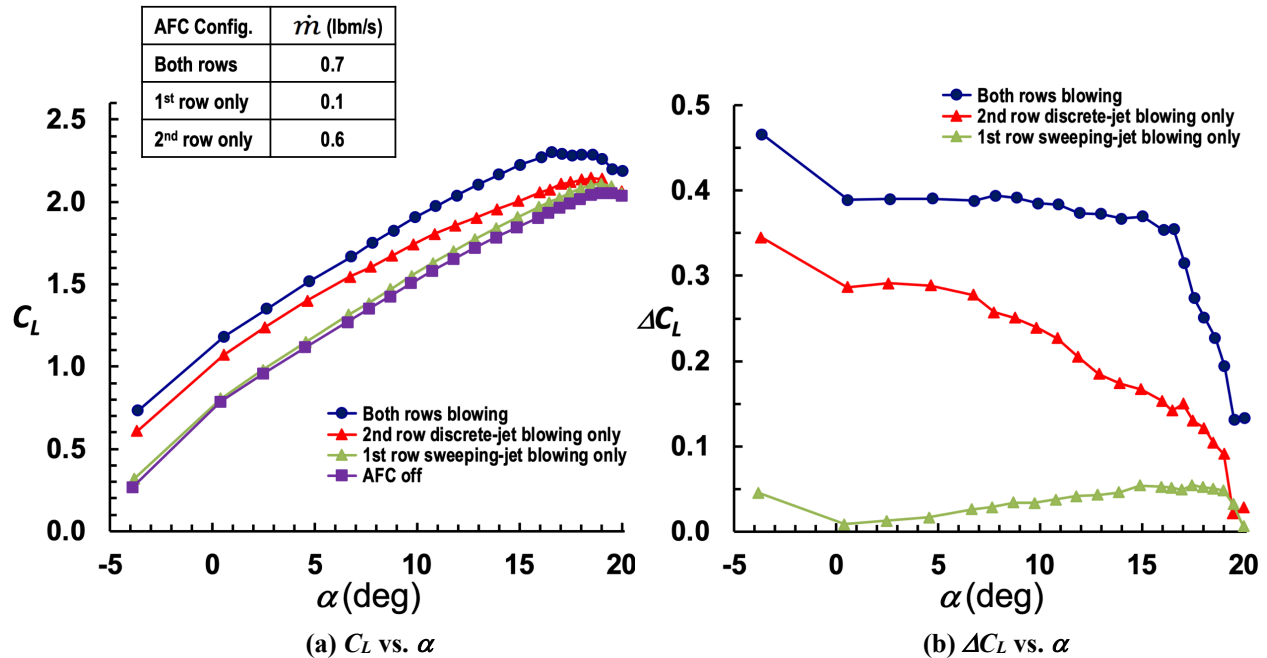


Fig. 6 Synergistic benefit of HELP actuation between 1<sup>st</sup> and 2<sup>nd</sup> rows (NPR = 1.5,  $M_\infty = 0.2$ ).

The lift curves produced by partial AFC coverage using up to eight HELP actuators (C1-C6, C1-C8, or C1-C4 plus C7-C8) with NPR = 2 and full coverage using all ten actuators (C1-C10) with NPR = 1.5 are shown in Fig. 7(a). The lift curve of the reference CRM-HL, defined in Ref. [7] as the configuration with the engine nacelle and nacelle

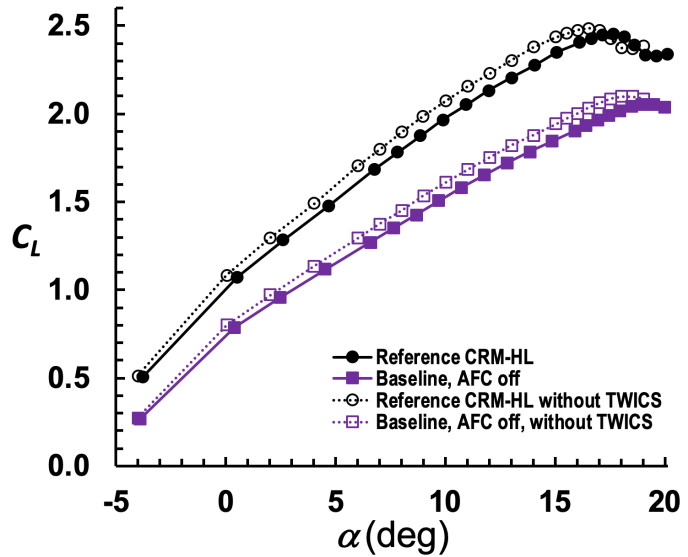


Fig. 5 Effect of tunnel wall corrections (TWICS) on the CRM-HL lift curves.

chine, is also plotted in the figure for comparative purposes. The reference CRM-HL lift curve has a slightly steeper slope compared to those of the CRM-SHL-AFC configurations, which present extra challenges for AFC at higher angles of attack. Although all of these AFC cases were able to match or exceed the lift performance of the reference CRM-HL at lower angles of attack (e.g.,  $\alpha \leq 6^\circ$ ), their lift performance fall significantly short of the reference case near the maximum lift ( $\alpha \approx 17^\circ$ ), as shown in Fig. 7(a).

In order to achieve the lift performance enhancement goal of  $\Delta C_L \geq 0.5$  at both lower angles of attack and near maximum lift (stall), ten HELP actuators with  $NPR \geq 2$  or eight actuators with  $NPR \approx 2.4$  were required to meet the lift performance goal, as shown in Fig. 7(b). One additional approach was taken in an attempt to reduce the mass flow usage of the HELP actuators by applying more pneumatic power over the inboard flap than over the outboard flap using a spanwise tailoring of NPR approach — typically NPR is  $\sim 1.3$  times its averaged value for C1 to C4 and  $\sim 0.7$  times its averaged value for C5 to C10. This approach also met our targeted lift performance goal at the lower angles of attack and came very close to reach the performance goal near maximum lift. The AFC-induced  $\Delta C_L$  increment was maintained for the entire lift curve that includes both lower angles of attack (e.g.,  $\alpha \approx 9^\circ$ ) and near maximum lift (i.e.,  $\alpha \approx 17^\circ$ ) for most cases examined. Note that  $9^\circ$  and  $17^\circ$  angles of attack are equivalent to  $8^\circ$  and  $16^\circ$ , respectively, without the tunnel wall corrections applied. As shown in Fig. 7(b), full HELP actuation coverage (C1-C10) with  $NPR \approx 2.4$  was able to exceed the lift performance of the reference conventional CRM-HL for the entire angle of attack range, thereby fulfilling the lift enhancement goal.

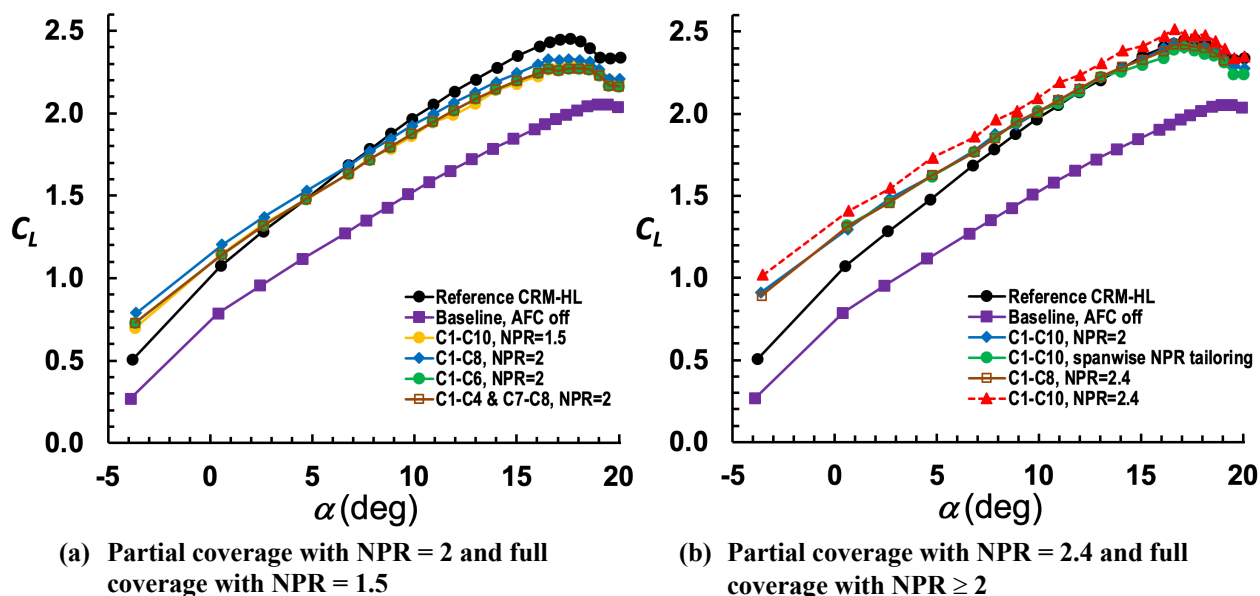


Fig. 7 Comparison of lift curves between various HELP actuations ( $M_\infty = 0.2$ ).

For completeness, the drag polar and pitching moment characteristics are shown in Figs. 8(a) and 8(b), respectively, for the cases of partial coverage with  $NPR = 2.4$  and full coverage with  $NPR \geq 2$  shown in Fig. 7(b). As expected, the higher flap deflections ( $50^\circ/55^\circ$ ) of the CRM-SHL-AFC configuration produced higher drag compared to the reference CRM-HL case with a lower flap deflection ( $37^\circ$ ) as shown in Fig. 8(a). The most effective HELP actuation (full coverage at  $NPR = 2.4$ ) generally produced slightly lower drag for the same lift, but it might produce more induced drag (drag due to lift) at higher  $\alpha$ . It should be noted that the increase in drag without losing the lift for the landing configuration could be desirable whenever a substantial speed reduction of the aircraft is required.

Figure 8(b) shows that the  $C_m$  is negative for all cases examined, and the most effective HELP actuation (liftwise) produced the  $C_m$  performance closest to the reference CRM-HL. A negative  $C_m$  (or nose-down pitching moment) helps to maintain aircraft longitudinal stability. The AFC off case of the CRM-SHL-AFC has the least amount of negative  $C_m$ . All  $C_m$  curves have positive slopes between  $\alpha = 0^\circ$  and  $\alpha \approx 18^\circ$ . Compared to the reference CRM-HL, the trends for all AFC cases show a slightly steeper (more positive) slope for  $\alpha < 18^\circ$ . This is because the Fowler flap of the reference case has a longer moment arm to the moment center than the simple-hinged flap (due to the flap extension and lower flap deflection), therefore, the suction pressures on flap produced more nose-down pitching moment (negative  $C_m$ ) at higher angles of attack.

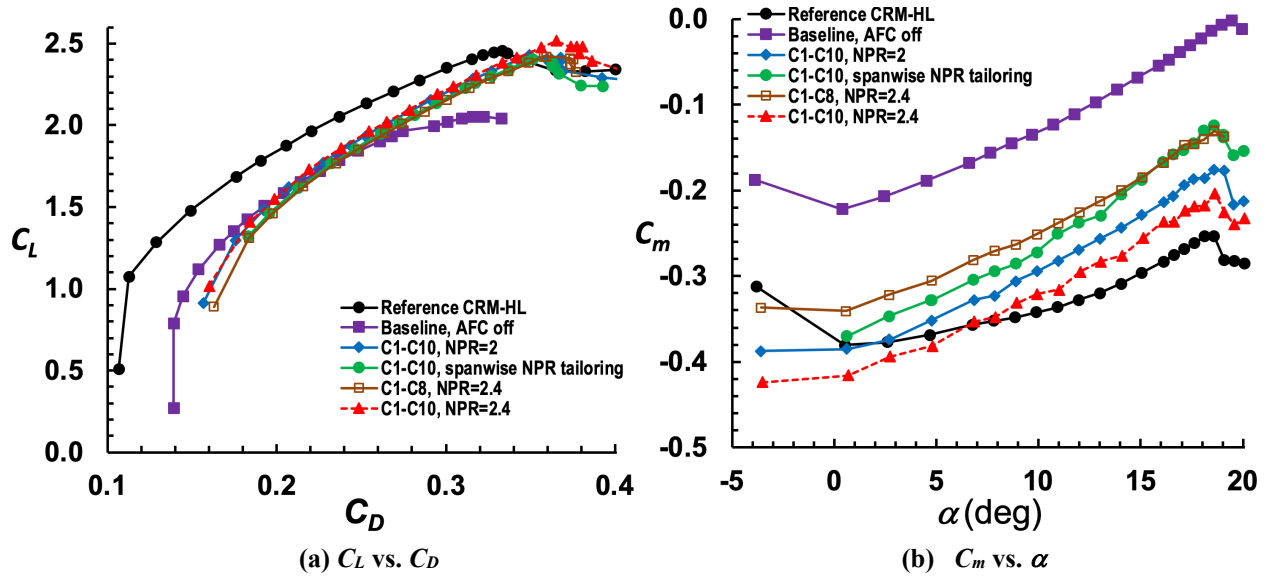


Fig. 8 Comparison of drag polar and pitching moment between various HELP actuations ( $M_\infty = 0.2$ ).

### B. Pneumatic Power Usage

The two key angles of attack for high-lift design,  $\alpha = 9^\circ$  in the linear region of the lift curve and  $\alpha = 17^\circ$  near the maximum lift, were selected for comparison in terms of pneumatic power usage requirements. Figure 9 shows the effects of NPR on lift for various HELP actuations that were able to meet or come within 0.05  $\Delta C_L$  of the targeted lift performance goal for  $\text{NPR} \geq 2$ . The goal is indicated by the dotted line representing the lift levels of the reference CRM-HL. An NPR greater than  $\sim 1.8$  is needed to achieve the lift enhancement goals for  $\alpha = 9^\circ$  and an NPR greater than  $\sim 2.3$  is needed for  $\alpha = 17^\circ$ . Note that  $\text{NPR} = 1.8929$  corresponds to the choked flow condition. Based on the NPR requirement, HELP actuation with eight cartridges (C1-C8) is less efficient than activation of all ten cartridges for either constant spanwise NPR or spanwise NPR tailoring for both angles of attack (Fig. 9). However, the full span coverage of HELP actuators (C1-C10) with a constant spanwise NPR is the most effective because it is the only AFC case that is able to achieve the lift enhancement goal near stall ( $\alpha = 17^\circ$ ), as shown in Fig. 9(b).

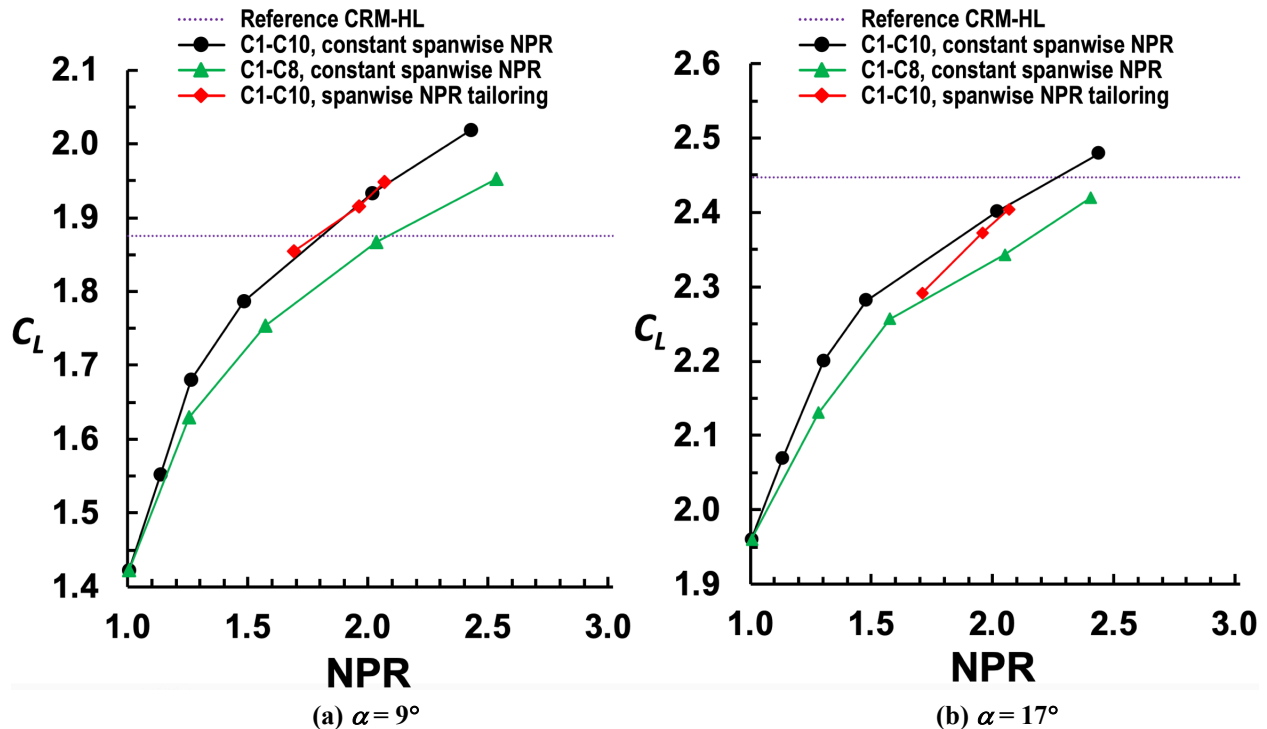


Figure 9.  $C_L$  versus NPR comparison between various HELP actuations ( $M_\infty = 0.2$ ).

Another important AFC parameter examined is the mass flow rate ( $\dot{m}$ ). Figure 10 presents the mass flow rate results for the selected angles of attack of  $9^\circ$  and  $17^\circ$ . Again, the dotted line marks the lift level of the reference CRM-HL, which represents the performance goal. The  $C_L$  versus  $\dot{m}$  curves roughly collapsed into a single curve and remained fairly linear for both  $\alpha = 9^\circ$  and  $\alpha = 17^\circ$ , which is a sign of good actuation efficiency. The spanwise tailoring of NPR that emphasizes more inboard blowing performed like the untailored case (constant spanwise NPR) at both angles of attack. For the most effective AFC case (C1-C10, constant spanwise NPR), a mass flow rate of greater than  $\sim 0.91$  lbm/s ( $C_Q = 0.0027$ ) is needed to achieve the lift enhancement goal of  $C_L = 1.88$  at  $\alpha = 9^\circ$ , whereas a mass flow rate of greater than  $\sim 1.23$  lbm/s ( $C_Q = 0.0036$ ) is needed to achieve the lift enhancement goal of  $C_L = 2.45$  at  $\alpha = 17^\circ$ .

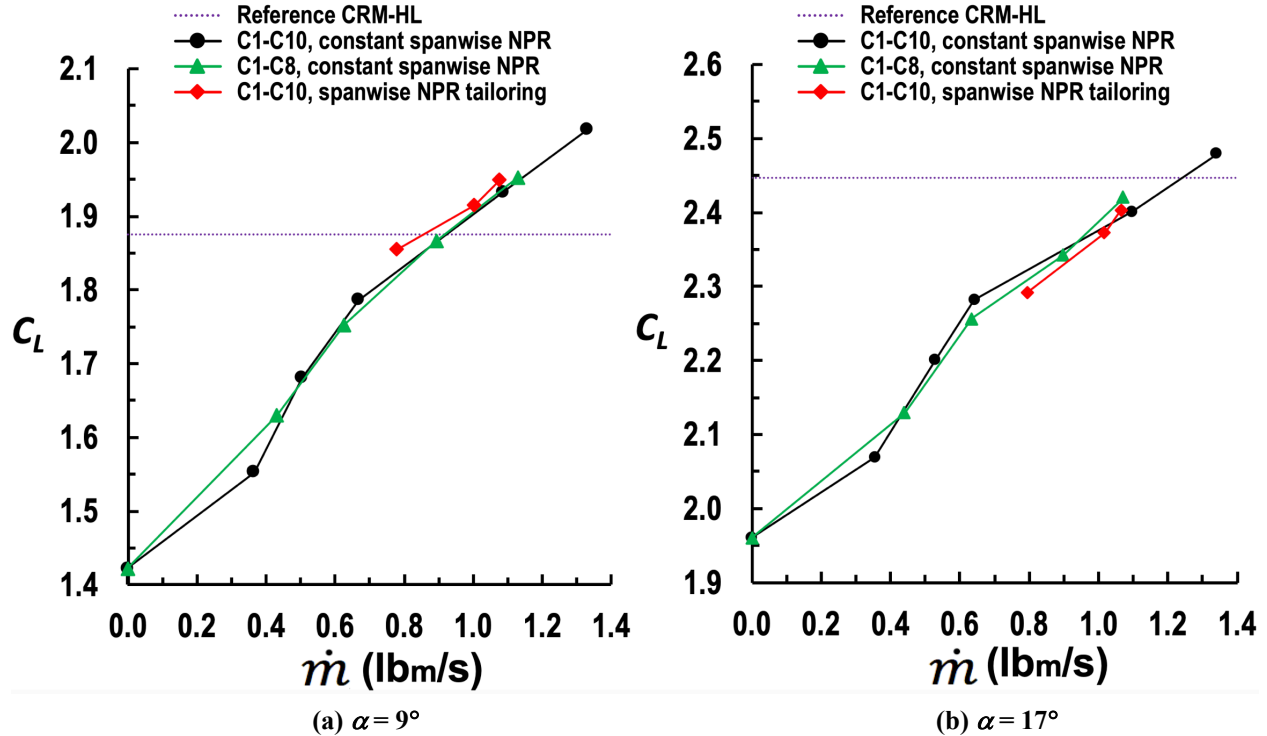


Figure 10.  $C_L$  versus  $\dot{m}$  comparison between various HELP actuations ( $M_\infty = 0.2$ ).

The momentum coefficient ( $C_\mu$ ) is a parameter that has been used for scaling up the performance of AFC actuators [22]. Figure 11 shows that a  $C_\mu$  of greater than  $\sim 0.025$  is needed for the most effective HELP actuation (C1-C10, constant spanwise NPR) to achieve the lift enhancement goal at  $\alpha = 9^\circ$ , and a  $C_\mu$  of greater than  $\sim 0.037$  is needed to achieve the lift enhancement goal at  $\alpha = 17^\circ$ . Lin et al. [7] suggested that the power coefficient ( $C_\pi$ ) is a better parameter to use for judging the performance efficiency of AFC actuators. The  $C_\pi$  takes account of both the mass flow rate (i.e.,  $C_Q$ ) and the supply air pressure (i.e., NPR). It is linked to the power usage of a pneumatic-based AFC system as described by Seele et al. [23]. For the most effective AFC case (C1-C10, constant spanwise NPR), the pneumatic power requirements that enable the HELP actuation to achieve the lift performance goals are  $C_\pi \approx 0.18$  and  $0.3$  for  $\alpha = 9^\circ$  and  $17^\circ$ , respectively. The trends and characteristics of the  $C_L$  versus  $C_\pi$  curves are somewhat similar to those of  $C_L$  versus  $C_\mu$  curves (Fig. 11). Both curves roughly collapsed into a single curve for both  $\alpha = 9^\circ$  and  $\alpha = 17^\circ$ , suggesting that  $C_\pi$  may be used for scaling up of a pneumatic-based AFC system such as the HELP actuation, because  $C_Q$  is scalable — and perhaps NPR too — from a system perspective.

There are no direct data on the scaling of  $C_\pi$  at the moment. However, the current 10%-scale CRM-HL model indicated a  $\Delta C_L$  of  $0.25$  at  $\alpha = 9^\circ$  ( $\sim 8^\circ$  uncorrected) corresponding to a  $C_\pi$  of about  $0.06$  for using the HELP actuators, which is very close to the full-scale test results of an AFC-enabled vertical tail for similar values of  $\Delta C_L$  and  $\alpha$  that required a corresponding  $C_\pi$  of about  $0.06$  [22]. Granted they are for different simple-hinged flap deflections ( $50^\circ$  for CRM-HL and  $30^\circ$  for the vertical tail), different wing planforms, and different types of actuators (HELP actuators for the former and sweeping jets for the latter); nevertheless, the agreement in  $C_L$  vs.  $C_\pi$  performance is surprisingly close. Therefore, it is perhaps reasonable to assume at this time, for system study and integration purposes, that the  $C_\pi$  is scalable.

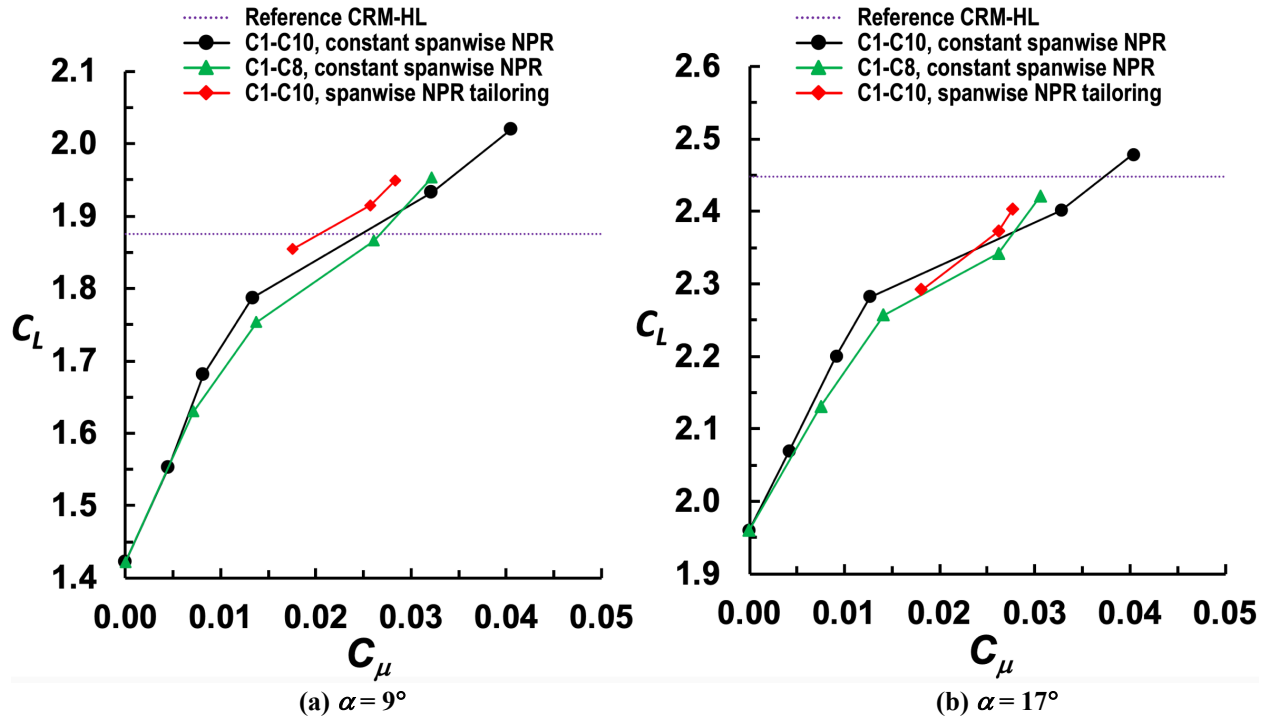


Figure 11.  $C_L$  versus  $C_\mu$  comparison between various HELP actuations ( $M_\infty = 0.2$ ).

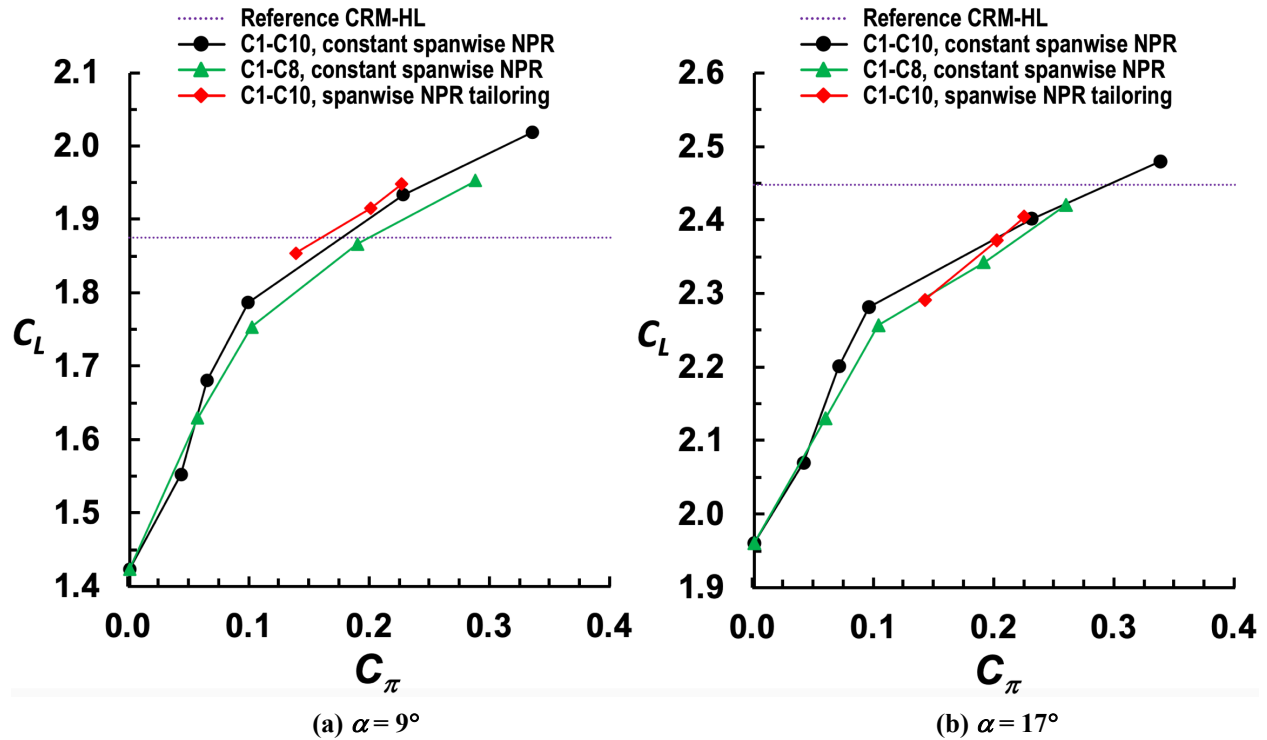


Figure 12.  $C_L$  versus  $C_\pi$  comparison between various HELP actuations ( $M_\infty = 0.2$ ).

### C. Surface Pressures and Flow Visualization

Three chordwise pressure coefficient ( $C_p$ ) distributions measured at approximately the station across the midspan of the inboard flap ( $y = 27.75$  inches), the midspan of the outboard flap ( $y = 63.8$  inches), and beyond the outboard flap ( $y = 94.7$  inches) are shown in Figs. 13, 14, and 15, respectively. Figure 2 and the inserts in each of the 3 figures illustrate their respective chordwise locations. Again, they are shown for various HELP actuations at the two selected angles of attack examined (i.e.,  $\alpha = 9^\circ$  and  $17^\circ$ ). Figures 13(a), 14(a), and 15(a) show the comparison for  $\alpha = 9^\circ$ , while Figs. 13(b), 14(b), and 15(b) show the comparison for  $\alpha = 17^\circ$ . Notice that the pressure tap locations in the  $x$ -direction are in deflected coordinates, however, their alignments at  $y$  stations of 27.75 inches, 63.8 inches, and 94.7 inches (inset images) are based on the stowed configuration because the deflected  $y$  coordinates for the slats and flaps are not in alignment with the freestream direction.

The results of the reference CRM-HL (conventional high-lift configuration with engine nacelle and nacelle chine) [7] are also included in the figures for comparison. Generally speaking, the HELP actuation produced more lift, on the slats and the main wing, whereas the reference CRM-HL ( $37^\circ$  conventional flaps) produced higher suction pressures on the outboard flaps. The CRM-HL shows no sign of flow separation on the inboard flap (Fig. 13) but displays flow separation at  $\sim 60\%$  of the outboard flap chord (Fig. 14).

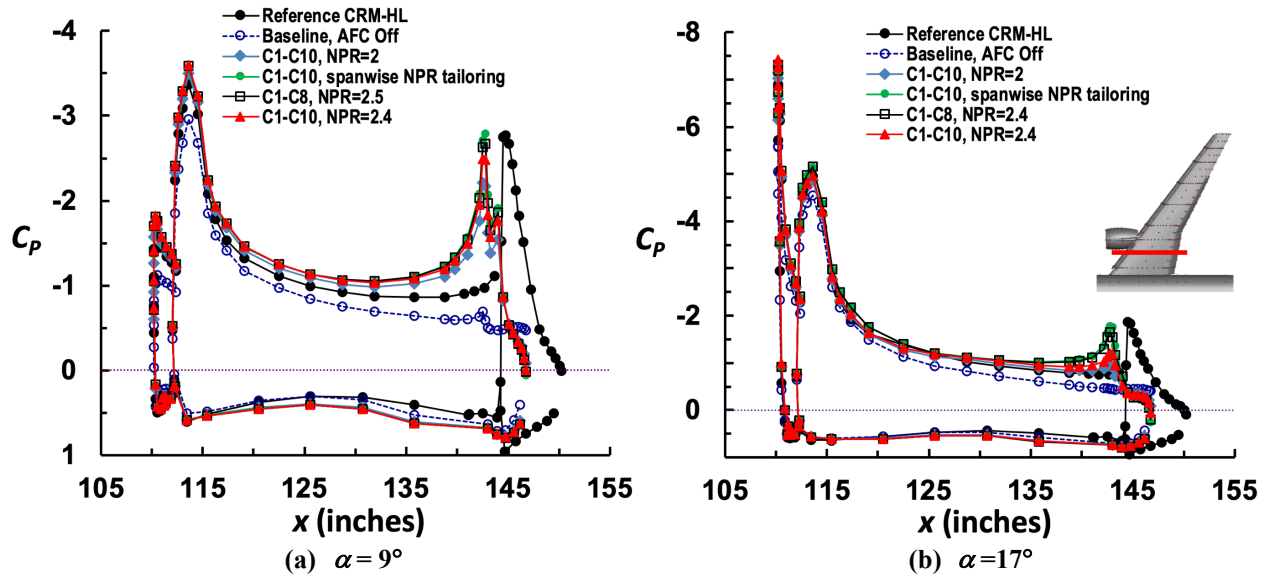


Figure 13.  $C_p$  distributions at  $y = 27.75$  inches for various HELP actuations ( $M_\infty = 0.2$ ).

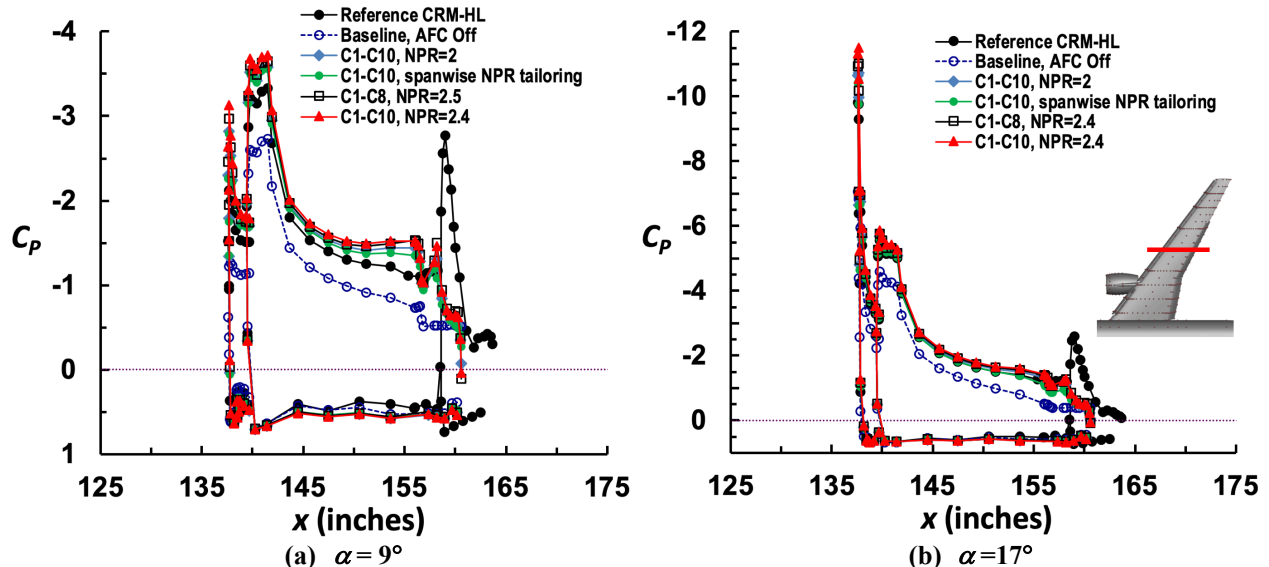


Figure 14.  $C_p$  distributions at  $y = 63.8$  inches for various HELP actuations ( $M_\infty = 0.2$ ).

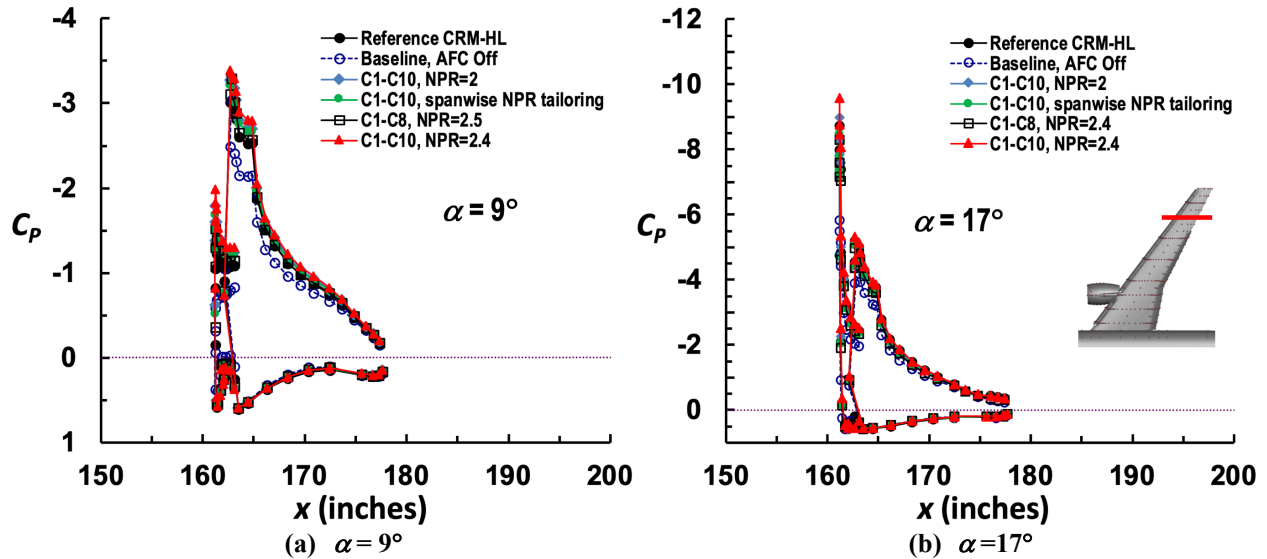


Figure 15.  $C_p$  distributions at  $y = 94.7$  inches for various HELP actuations ( $M_\infty = 0.2$ ).

The  $C_p$  distributions show that AFC significantly increased the suction pressure on the upper surfaces of the inboard and outboard slats, the main wing, and the inboard and outboard flaps over the baseline (AFC off) case. For the inboard flap station ( $y = 27.75$  inches) at  $\alpha = 9^\circ$ , the AFC-induced suction pressure increase near the flap hinge line is especially noticeable (Fig. 13(a)). The increase in suction pressure directly resulted in the increase in lift force observed for all HELP actuations. Also at the inboard station ( $y = 27.75$  inches), the spanwise tailoring of NPR and partial coverage with C1-C8 produce slightly more suction pressure around the flap shoulder than the uniform blowing at a maximum NPR of 2.4 (Fig. 13). However, the spanwise tailoring of NPR produces slightly less suction pressure at the outboard flap station (Fig. 14,  $y = 63.8$  inches). For the outboard wing or aileron station ( $y = 94.7$  inches), the AFC-induced increase in the suction pressures still remained on the slat and the wing leading edge at both  $\alpha$  values presented in Fig. 15, despite the fact that AFC actuation ended prior to this spanwise station. The CRM-HL model does not have a flap at the most outboard section and the pressure distributions show no evidence of flow separation near the wing trailing edge at this particular station (Fig. 15).

A maximum suction  $C_p$  of around -3.5 or greater was achieved on the main wing leading edge at  $\alpha = 9^\circ$  for all three spanwise ( $y$ ) stations. Perhaps due to the increase in flow circulation at  $\alpha = 17^\circ$ , substantially higher suction  $C_p$  values — approximately -7.4 for  $y = 27.75$  inches, -11.5 for  $y = 68.3$  inches, and -9.6 for  $y = 94.7$  inches are observed for the higher angle of attack case ( $\alpha = 17^\circ$ ) at the slat leading edge. Increased pressure recovery is also observed on the flap surfaces at both angles of attack. The pressure increase on the lower (nonactuated) surfaces is minimal for most cases at  $\alpha = 9^\circ$  and  $17^\circ$ .

The spanwise  $C_p$  distributions near the wing leading edge and midchord as well as the flap trailing edge of the CRM-SHL-AFC configuration with various HELP actuations at  $\alpha = 9^\circ$  and  $17^\circ$  are presented in Figs. 16(a) and 16(b), respectively. The results of the reference CRM-HL are also shown for comparison. For clarity, the top image shows the location of the spanwise pressure rows. The locations of the nacelle pylon, the yehudi break, and the outboard flap edge are illustrated by dotted vertical lines in the figure. The effect of the engine nacelle is clearly shown in the  $C_p$  distributions for the wing leading-edge row. The drop in the suction pressure at  $y = 38$  inches is due to the wake (i.e., velocity deficit) generated by the nacelle pylon. The nacelle wake footprint dissipates before the midwing row but the spanwise  $C_p$  distributions appear slightly skewed toward the outboard direction (Fig. 16).

The spanwise  $C_p$  distributions are mostly similar between  $\alpha = 9^\circ$  and  $17^\circ$  except for the higher suction pressure on the wing leading edge. On the other hand, the higher suction pressure over the wing midchord disappeared for the HELP actuation compared to the conventional CRM-HL for  $\alpha = 17^\circ$ . Various HELP actuations with  $\text{NPR} \geq 2$  all had similar spanwise pressure distributions over the wing; but the best performing case remains the activation of all actuators (C1-C10) at a constant spanwise NPR of 2.4. As expected, all AFC cases provided higher spanwise suction pressures along the wing leading edge and also better pressure recovery on the flap trailing edge at both  $\alpha = 9^\circ$  and  $17^\circ$  compared to the baseline case. The AFC-induced suction pressure increase extends all the way to the wingtip, perhaps benefiting from the wing sweep ( $35^\circ$  on the leading edge). The increase in spanwise suction pressures is especially notable on the wing leading edge, well past the  $y$  location of the outboard flap edge where AFC actuation ends for both angles of attack.

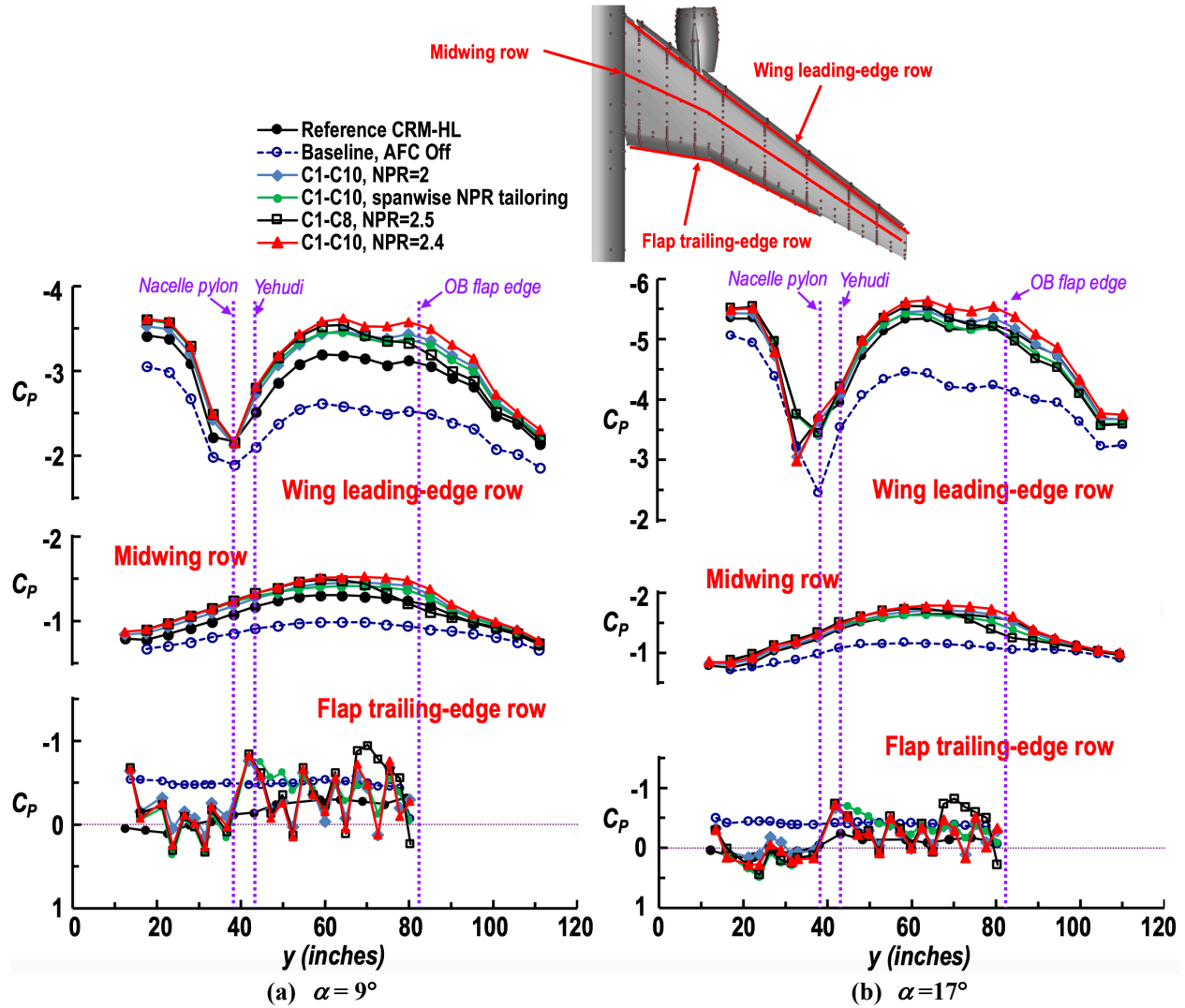
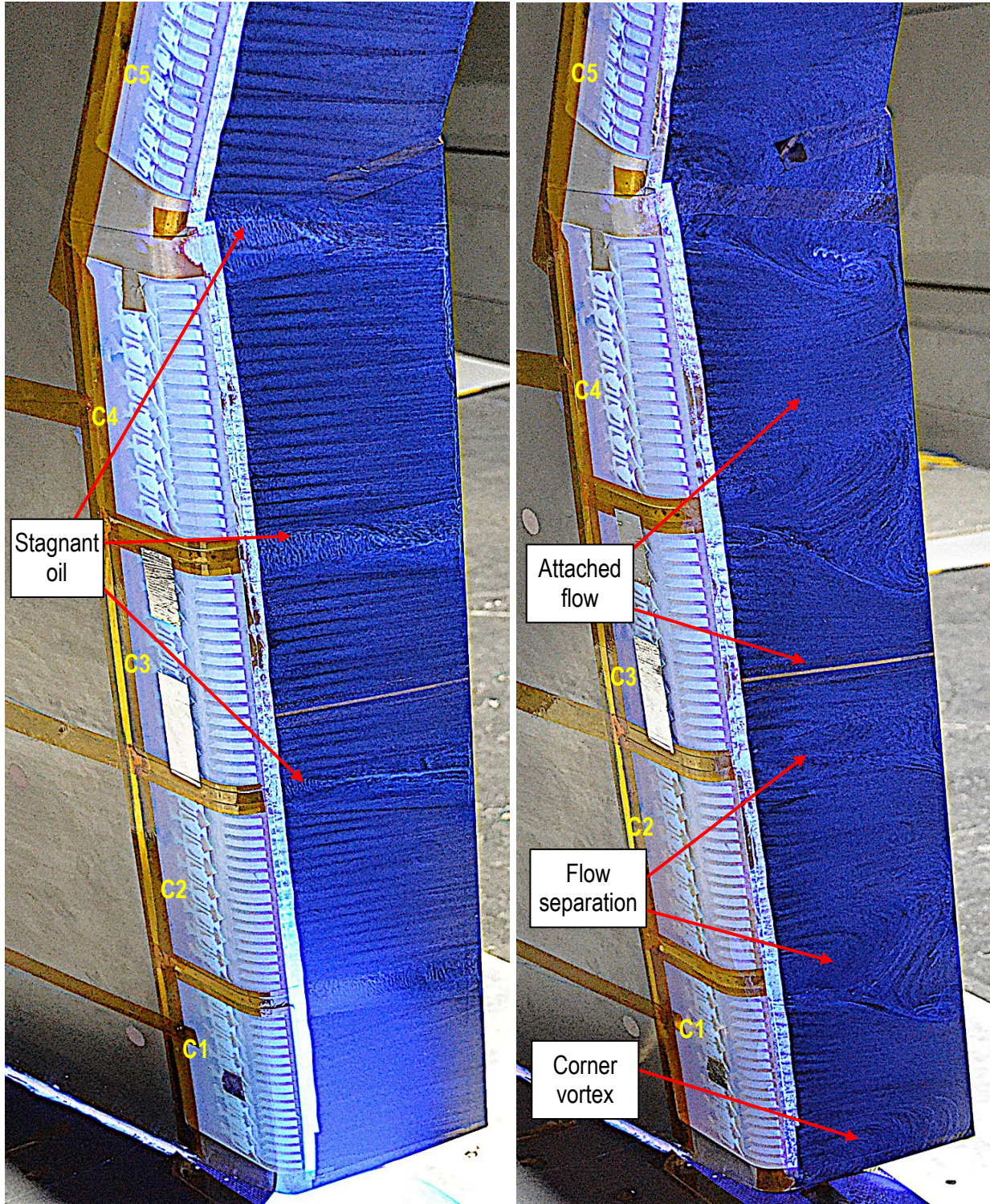


Figure 16. Spanwise  $C_p$  distributions for various HELP actuations ( $M_\infty = 0.2$ ).

The trailing-edge spanwise  $C_p$  distribution results indicate that the flow over the flaps is much more three dimensional (3D) for the AFC cases than either the baseline (AFC off) case or the reference CRM-HL case. The AFC-induced periodicity in the  $C_p$  distributions roughly matches the number of AFC cartridges ( $\sim 10$ ) and their averaged pressure values are generally approaching that of the reference CRM-HL. Both spanwise tailoring and the C1-C8 actuation approach are slightly less effective on the outboard flap for flow control. Generally speaking, AFC with the HELP actuation on the flap shoulder increased the suction pressures (and flow circulation) globally, in both the streamwise and the spanwise directions, and thereby enhanced the lift over the entire high-lift system.

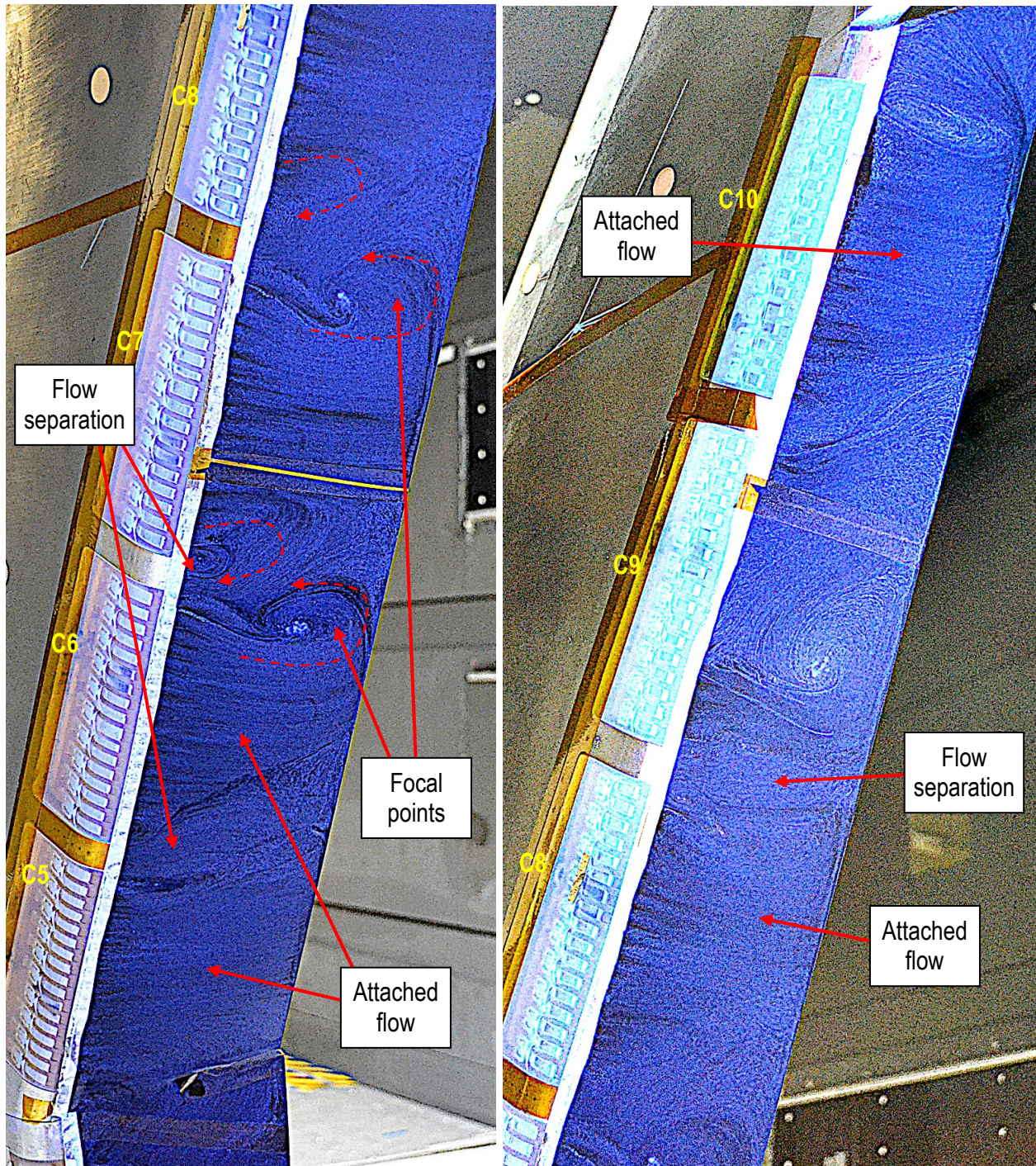
Figures 13 to 16 show that the HELP actuation with  $NPR \geq 2$  all had similar pressure distributions over the high-lift system; therefore, only the best performing case (C1-C10, constant spanwise NPR of 2.4) was selected for surface oil flow to further visualize and qualify the flow physics associated with AFC on the flap at  $\alpha = 9^\circ$  (with TWICS applied). Figure 17(a) shows the oil flow visualization of the actuator jet flow on the inboard flap without any freestream flow in the wind tunnel. The flow visualization indicates that the jets out of actuator cartridges are tangent to the flap surface without generating any unexpected flow pattern. However, there is stagnant oil downstream of the gaps between actuator cartridges. Consequently, local flow separation developed at these nonactuated regions on the flap (i.e., downstream of the gaps between actuator cartridges) when the tunnel flow was on, as shown in Fig. 17(b). The figure shows that HELP actuators maintained the attached flow over most of the flap surface. For the outboard flap, similar to the inboard flap, attached and separated flow patterns were observed for both the inboard and outboard regions, as shown in Figs. 18(a) and 18(b), respectively. However, the strong spanwise flow on the outboard flap created asymmetric focal points that can be clearly observed in Fig. 18(a). These locally separated and attached flow regions compare well with the spanwise variations in the trailing-edge static pressures (Fig. 16(a)).



(a) Inboard flap ( $M_\infty = 0$ )

(b) Inboard flap ( $M_\infty = 0.2$ )

Figure 17. Oil flow visualization of the HELP actuation on the inboard flap at NPR = 2.4 and  $\alpha = 9^\circ$ .



(a) Inboard region of outboard flap ( $M_\infty = 0.2$ )

(b) Outboard region of outboard flap ( $M_\infty = 0.2$ )

Figure 18. Oil flow visualization of the HELP actuation on the outboard flap at NPR = 2.4 and  $\alpha = 9^\circ$ .

These periodic 3D flow features (locally separated and attached flow regions) on the flaps were predicted by the CFD results reported by Vatsa et al. [8] as shown in Fig. 19. Although the gaps between the AFC cartridges could not be eliminated due to model structural considerations, the partial flow attachment induced by the HELP actuators was still able to provide sufficient lift enhancement for the CRM-SHL-AFC to meet its performance goal — i.e., to match or exceed the lift performance of the reference conventional high-lift configuration, CRM-HL equipped with a nacelle chine.

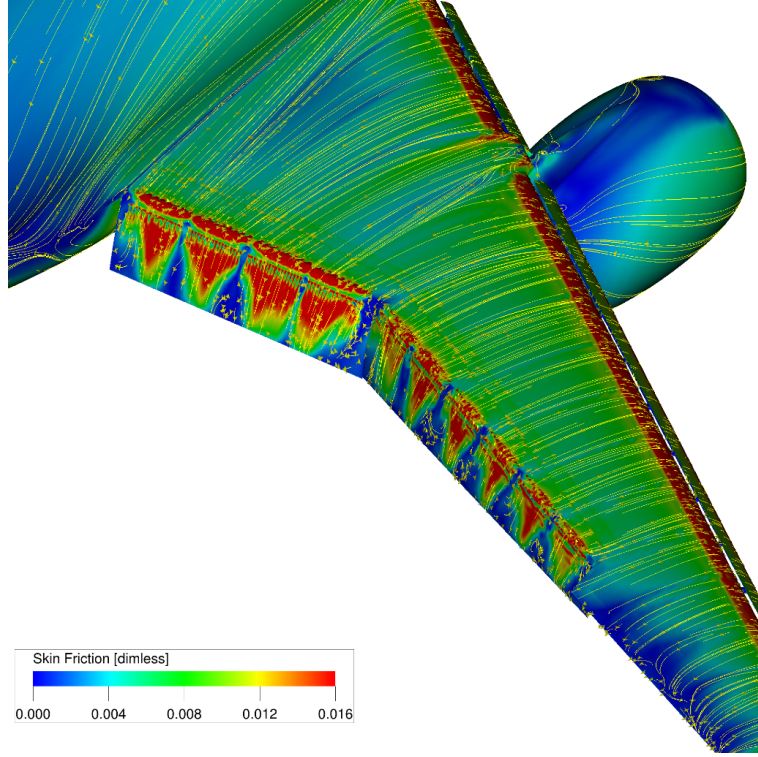


**Figure 19. Simulated surface streamline with activation of all HELP actuators (C1-C10) at NPR = 2.4 and  $\alpha = 9^\circ$  (equivalent to TWICS applied) from Vatsa et al. [8].**

## V. Conclusions

A High Efficiency Low Power (HELP) methodology has been successfully developed and tested on an active flow control (AFC) version of the high-lift version of the Common Research Model (CRM-SHL-AFC) at the NASA Langley Research Center 14- by 22-Foot Subsonic Tunnel (14x22). The HELP actuators, which use a combination of unsteady sweeping jets and steady discrete jets in tandem, were designed to overcome strong adverse pressure gradients, while minimizing the pneumatic power usage. Leveraging on the synergistic benefit of tandem rows, the HELP actuation enables the Row 1 sweeping jet to provide an effective Coanda boost to the Row 2 discrete jets that resulted in strong flow-control authority. The AFC-induced  $\Delta C_L$  enhancement was maintained for the entire lift curve for most flow control cases examined. Because the reference CRM-HL configuration has a Fowler flap, its lift curve has a slightly steeper slope compared to the CRM-SHL-AFC configuration. This presents extra challenges for AFC at higher angles of attack (e.g., near maximum lift) where more pneumatic power is required to achieve the lift performance goal.

Although ten HELP actuators with  $NPR \geq 2$  and eight actuators with  $NPR = 2.4$  were able to produce the lift coefficient increases (i.e.,  $\Delta C_L \approx 0.5$ ) required to match the lift goal of  $C_L = 1.88$  at the lower angle of attack case ( $\alpha = 9^\circ$ ), all ten actuators with a constant spanwise NPR of 2.4 were required to achieve the lift goal of  $C_L = 2.45$  near the maximum lift ( $\alpha = 17^\circ$ ). For the most effective AFC case (i.e., C1-C10, constant spanwise NPR), mass flow rates greater than  $\sim 0.91$  lbm/s and NPR values greater than  $\sim 1.8$  (corresponding to  $C_\pi = 0.18$ ,  $C_Q = 0.0027$ , and  $C_\mu = 0.025$ ) are needed to achieve the lift enhancement goal at  $\alpha = 9^\circ$ , whereas mass flow rates greater than  $\sim 1.23$  lbm/s and NPR values greater than  $\sim 2.3$  (corresponding to  $C_\pi = 0.3$ ,  $C_Q = 0.0036$ , and  $C_\mu = 0.037$ ) are needed to achieve the lift enhancement goal at  $\alpha = 17^\circ$ . The power coefficient ( $C_\pi$ ), which takes into account both supply air pressure and mass flow usage for the AFC actuators, is a useful parameter for judging the actuators' performance efficiency and perhaps can be used for scaling-up the AFC system.

Surface pressures and oil flow visualization were used to analyze the effects and impacts of the HELP actuation in order to better understand the relevant flow physics. Surface pressure distributions indicate that AFC with the HELP actuation on the flap shoulder increased the suction pressures (and flow circulation) globally, in both the streamwise and the spanwise directions, and thereby enhanced the lift over the entire high-lift system. The surface oil flow visualization indicated 3D and periodic flow features (i.e., locally separated and attached flow regions), which were also predicted by numerical simulations (Vatsa et al. [8]). Although the gaps between the AFC cartridges could not be eliminated due to structural considerations, the partial flow attachment induced by the HELP

actuators was still able to provide significant lift enhancement for the CRM-SHL-AFC. Ultimately, the CRM-SHL-AFC configuration equipped with HELP actuation was able to match or exceed the lift performance of the reference conventional high-lift configuration (i.e., CRM-HL equipped with a nacelle chine), thus meeting the objective of the research.

### Acknowledgments

This R&D effort was sponsored by the High Aspect Ratio Wing Subproject under the NASA Advanced Air Transport Technology (AATT) Project. The effort involved many people who provided valuable contributions through their hard work that made a successful test possible. The authors would like to acknowledge and thank all those involved for their great support during the course of this investigation. Some key personnel are as follows.

*Model design:* Jared Fell (design team lead), Sandy Webb, Miranda Snyder, Christopher Laws, Reggie Kidd, John Mulvaney, Mark Cagle, David Lewis, Nigel Schneider, Dave Castle, Douglas Weber, William Langford, and Ray Rhew, as well as NASA interns Jacob Ganzak and Steven Call.

*Model fabrication:* Stephen Geissinger, Christopher Mclain, Danny Lovaglio, Robert Andrew, and Thomas Hall.

*14x22 air supply system and AFC plumbing:* Joe Giuliana.

*14x22 managerial staff:* Frank Quinto (Facility Manager), Ashley Dittberner (Operation Manager), William Krieger (Facility Safety Head), Joseph Burton (Facility Coordinator).

*14x22 Test Engineers:* James Byrd (Lead), Abigail Cayton, Jeremy Ulanday, and Samantha Zauber.

*14x22 technician and supporting staff:*

Lead Technician - Ronald Hunter

Mechanical Technicians - Kyle Deaver (Lead), Joshua Beasley, Marvin Le Gendre, Andrew Sawyer, Cassandra Stevens, and Patricia Christian

Instrumentation Technician - Andrew Harrison, Benjamin Lester, and Neil Coffey

Electrical Technician - Stuart Dale Bennett and Leon Adams

Data System - Andy Boney (Manager), Benjamin Trower, and Charlotte Teague

Facility Equipment Specialist - Karl Maddox

Environmental Coordinator - Joseph Burton, Jr.

High Pressure Air Support - Michael Henshaw and Robert Askew

*CRM-HL CFD data:* David Lockard and Melissa Rivers

*CRM-HL consultation:* Douglas Lacy of Boeing Commercial Airplanes

### References

- [1] Van Dam, C. P., "The Aerodynamic Design of Multi-Element High-Lift Systems for Transport Airplanes," *Progress in Aerospace Sciences*, Vol. 38, 2002, pp. 101–144. doi: 10.1016/S0376-0421(02)00002-7
- [2] Greenblatt, D. and Wynnanski, I. J., "The Control of Flow Separation by Periodic Excitation," *Progress in Aerospace Sciences*, Volume 36, Issue 7, 2000, pp. 487-545. doi: 10.1016/S0376-0421(00)00008-7
- [3] Cattafesta III, L. N. and Sheplak, M., "Actuators for Active Flow Control," *Annual Review of Fluid Mechanics*, Vol. 43, Issue 1, August 2010, pp. 247-272. doi:10.1146/annurev-fluid-122109-160634
- [4] McLean, J. D., Crouch, J. D., Stoner, R. C., Sakurai, S., Seidel, G. E., Feifel, W. M., and Rush, H. M., "Study of the Application of Separation Control by Unsteady Excitation to Civil Transport Aircraft," NASA/CR 1999–209338, 1999. <https://ntrs.nasa.gov/archive/nasa/casi.ntrs.nasa.gov/19990061938.pdf>
- [5] Hartwich, P. M., Camacho, P. P., El-Gohary, K., Gonzales, A. B., Lawson, E. L., and Shmilovich, A., "System-Level Trade Studies for Transonic Transports with Active Flow Control (AFC) Enhanced High-Lift Systems," *55th AIAA Aerospace Sciences Meeting*, AIAA Paper 2017-0321, 2017. doi: 10.2514/6.2017-0321
- [6] Shmilovich, A., Yadlin, Y., Dickey, E. D., Hartwich, P.M., and Khodadoust, A., "Development of an Active Flow Control Technique for an Airplane High-Lift Configuration," *55th AIAA Aerospace Sciences Meeting*, AIAA Paper 2017-0322, 2017. doi: 10.2514/6.2017-0322
- [7] Lin, J. C., Melton, L. P., Hannon, J. A., Andino, M. Y., Koklu, M., Paschal, K. B., and Vatsa, V. N., "Wind Tunnel Testing of Active Flow Control on the High Lift Common Research Model," *AIAA AVIATION 2019 Forum*, AIAA Paper 2019-3723, 2019. doi: 10.2514/6.2019-3723

- [8] Vatsa, V. N., Duda, B., Lin, J. C., Melton, L. P., Lockard, D. P., O’Connell, M., and Hannon, J. A., “Comparative Study of Active Flow Control Strategies for Lift Enhancement of a Simplified High-Lift CRM Configuration,” *AIAA AVIATION 2019 Forum*, AIAA Paper 2019-3724, 2019. doi: 10.2514/6.2019-3724
- [9] Melton, L. P., Lin, J. C., Hannon, J. A., Andino, M. Y., Koklu, M., and Paschal, K. B., “Sweeping Jet Flow Control on the Simplified High-Lift Version of the Common Research Model,” *AIAA AVIATION 2019 Forum*, AIAA Paper 2019-3726, 2019. doi: 10.2514/6.2019-3726
- [10] Koklu, M., Lin, J. C., Hannon, J. A., Melton, L. P., Andino, M. Y., Paschal, K. B., and Vatsa, V. N., “Surface Flow Visualization of the High-Lift Common Research Model,” *AIAA AVIATION 2019 Forum*, AIAA Paper 2019-3727, 2019. doi: 10.2514/6.2019-3727
- [11] Jones, G. S., Milholen, W. E., II, Chan, D. T., Melton, L. P., Goodliff, S. L., and Cagle, C. M., “A Sweeping Jet Application on a High Reynolds Number Semispan Supercritical Wing Configuration,” *35th AIAA Applied Aerodynamics Conference*, AIAA Paper 2017-3044, 2017. doi: 10.2514/6.2017-3044
- [12] Gentry, G. L., Quinto, F. P., Gatlin, G. M., Applin, Z. T. “The Langley 14- by 22-Foot Subsonic Tunnel: Description, Flow Characteristics, and Guide for Users,” NASA-TP-3008 September, 1990. <https://ntrs.nasa.gov/search.jsp?R=19900018333>
- [13] Vassberg, J. C., DeHaan, M. A., Rivers, S. M., and Wahls, R. A., “Development of a Common Research Model for Applied CFD Validation Studies,” *26th AIAA Applied Aerodynamics Conference*, AIAA Paper 2008-6919, 2008. doi: 10.2514/6.2008-6919
- [14] NASA Common Research Model, December 2017. <http://commonresearchmodel.larc.nasa.gov>
- [15] Rivers, M. B., “NASA Common Research Model: A History and Future Plans,” *AIAA AVIATION 2019 Forum*, AIAA Paper 2019-3725, 2019. doi: 10.2514/6.2019-3725
- [16] Lacy, D. S. and Sclafani, A. J., “Development of the High Lift Common Research Model (HL-CRM): A Representative High Lift Configuration for Transonic Transports,” *54th AIAA Aerospace Sciences Meeting*, AIAA Paper 2016-0308, 2016. doi: 10.2514/6.2016-0308
- [17] Third AIAA CFD High Lift Prediction Workshop, NASA HL-CRM Geometry Files, July 2016. <https://hilitpw.larc.nasa.gov/Workshop3/geometries.html>
- [18] Melton, L. P., Koklu, M., Andino, M., and Lin, J. C., “Sweeping Jet Optimization Studies,” *8th AIAA Flow Control Conference*, AIAA Paper 2016-4233, 2016. doi: 10.2514/6.2016-4233
- [19] Ulbrich, N., “The Real-Time Wall Interference Correction System of the NASA Ames 12-Foot Pressure Wind Tunnel,” NASA/CR – 1998-208537, July 1998.
- [20] Ulbrich, N. and Boone, A. R., “Real-Time Wall Interference Correction System of the 12-Foot Pressure Wind Tunnel,” AIAA Paper 98-0707, 1998. doi: 10.2514/6.1998-707
- [21] Iyer, V., Kuhl, D. D., and Walker, E. L., “Improvements to Wall Corrections at the NASA Langley 14X22-Foot Subsonic Tunnel,” AIAA Paper 2003-3950, 2003. doi: 10.2514/6.2003-3950
- [22] Lin, J. C., Whalen, E. A., Andino, M. Y., Graff, E. C., Lacy, D. S., Washburn, A. E., Gharib, M., and Wagnanski, I. J., “Full-Scale Testing of Active Flow Control Applied to a Vertical Tail,” *Journal of Aircraft*, 2019, accessed January 29, 2019. doi: <http://arc.aiaa.org/doi/abs/10.2514/1.C034907>
- [23] Seele, R., Graff, E., Lin, J., and Wagnanski, I., “Performance Enhancement of a Vertical Tail Model with Sweeping Jet Actuators,” *51st AIAA Aerospace Sciences Meeting*, AIAA Paper 2013-0411, 2013. doi: 10.2514/6.2013-411